Original Research Article

Histopathological parameter and brain tumor mapping using distributed optimizer tuned explainable AI classifier

Prasad R. Mutkule[1,*], Nilesh P. Sable[2], Parikshit N. Mahalle[3], Gitanjali R. Shinde[4]

[1] Department of Computer Engineering, Bansilal Ramnath Agarwal Charitable Trust's, Vishwakarma Institute of Information Technology, Savitribai Phule Pune University, Pune 411048, Maharashtra, India

[2] Department of Computer Science & Engineering (Artificial Intelligence), Bansilal Ramnath Agarwal Charitable Trust's, Vishwakarma Institute of Information Technology, Savitribai Phule Pune University, Pune 411048, Maharashtra, India

[3] Department of Artificial Intelligence & Data Science, Bansilal Ramnath Agarwal Charitable Trust's, Vishwakarma Institute of Information Technology, Savitribai Phule Pune University, Pune 411048, Maharashtra, India

[4] Department of Computer Science & Engineering (Artificial Intelligence & Machine Learning), Bansilal Ramnath Agarwal Charitable Trust's, Vishwakarma Institute of Information Technology, Savitribai Phule Pune University, Pune 411048, Maharashtra, India

* Corresponding author: Prasad R. Mutkule, mutkuleprasad000@gmail.com

ABSTRACT

Brain tumors represent a critical and severe challenge worldwide early and accurate diagnosis is necessary to increase the predictions for individuals with brain tumors. Several studies on brain tumor mapping have been conducted recently; however, the methods have some drawbacks, including poor image quality, a lack of data, and a limited capacity for generalization ability. To tackle these drawbacks this research presents a distributed optimizer tuned explainable AI classifier model for brain tumor mapping from histopathological images. The foraging gyps africanus optimization enabled explainable artificial intelligence (FGAO enabled explainable AI) combines the advantages of the explainable AI classifier model and hybrid spatio-temporal attention-based ResUNet segmentation model. The hybrid spatio-temporal attention-based ResUNet segmentation model accurately segments the histopathological images that leverage both Spatio-Temporal attention and the ResUNet model which addresses performance degradation problems. The nature-inspired algorithms draw inspiration from the foraging and hunting traits which optimize the tunable parameters of the explainable AI classifier. The SHAP model in the explainable AI translates the insights into predictions that produce explanations for the decisions made by the CNN model which fosters end-user confidence. The experimental results show that the FGAO-enabled explainable AI model outperforms the conventional approaches in terms of accuracy 95.75%, sensitivity 95.10%, and specificity 96.32% for TP 80.

Keywords: brain tumor mapping; explainable AI classifier; hybrid spatio-temporal attention-based ResUNet segmentation; foraging gyps africanus optimization; SHapley Additive exPlanations

1. Introduction

According to statistics, brain tumors rank as the tenth leading cause of death for both men and women[1] which arises when aberrant cells in the brain or spinal cord begin to develop unnecessarily. Based on histology and genetic characteristics, the World Health Organization (WHO) classified brain tumors in 2016 into four grades (I, II, III, and IV), ranging from low to high grade[2,3]. When the tumor is at a more advanced stage, the prognosis for brain cancer is minimal[4]. Thus, timely and precise cancer

diagnosis and grade estimation contribute to better disease prognosis and treatment planning. The main tests for tumor diagnosis and grade estimation include neurological examination, imaging, biopsies, and biomarkers[5]. When a tumor is small in the primary stage, which is referred to as benign[6]. When a tumor reaches the secondary stage it is referred to as malignant since it has grown beyond benign boundaries and is greater in size[7]. Numerous techniques are employed to treat brain tumors[8], radiation therapy is helpful in the benign stage, and a patient can live without surgery[9]. Conversely, the malignant stage is dangerous and responds well to radiotherapy and chemotherapy[10].

Computer-aided cancer diagnosis and grading systems rely heavily on the segmentation of histological images into meaningful segments. In the medical image domain, imaging segmentation is used to divide an image into two sections. The act of spitting out an image results in its being separated into portions, which enhances its representation and increases analytically usefulness. However, this could be a difficult problem to tackle because medical images often contain minor differences, certain types of noise, and absent or contested barriers. Computed tomography (CT) and magnetic resonance imaging (MRI) can be used to study the interior structure of the brain. Compared with CT images MRI scans are more valuable since they provide information on the texture and structure of the tumor[11]. The position, dimensions, and form of the detective tissues can be readily determined by MRI. A few drawbacks of these methods include their high cost and computation time[12]. Diverse investigators have offered distinct approaches for categorizing brain tumors. Image segmentation has been applied to the identification of anomalous brain tumors in several contexts. Individual MRI tumor imaging investigations require various algorithms for patient-specific training dataset. Accurate image segmentation, or fully automatic extract segmentation, is one of the open challenges.

Deep learning (DL) approaches have recently been investigated for the segmentation of histology images and have shown better results than previous techniques. Using a deep CNN and transfer learning[13] extracted features that an SVM classifier used to segment images of the brain's histology[14]. Even though the DL models were effective in learning features they typically need a large set of training images and related annotations, which can be challenging to collect the data images due to the tissue structures. To tackle this issue high-resolution histopathological image analysis has recently been made possible by advancements in digital pathology, giving researchers access to additional information from CAD image analysis which enables the full slide image to display precise quantitative histomorphometry features, such as histologic primitives (such as glands and nuclei) from a typical hematoxylin and eosin (H & E) slide[15]. A recent study improved diagnostic accuracy and shortened the screening time for prostate cancer by applying the contouring of various cells from histopathology images[16]. The traditional approaches such as SVM, ANN, DCNN, and LSTM have some limitations including high levels of anatomical diversity, image quality concerns, and the requirement for domain-specific expert interpretation.

Key contribution of the paper:

The key contribution of this paper is to introduce a brain tumor mapping model using FGAO-enabled explainable AI. The hybrid spatio-temporal attention-based ResUNet segmentation utilized in this paper minimizes the vanishing gradient problems and produces accurate segmented brain tumor histopathological images. The Spatio-Temporal ResNet features enhance the feature extraction capacity of the proposed model which leads to precise mapping of brain tumors. The explainable AI classifier incorporates the advantages of an explainable mechanism along with the CNN model that accurately maps the brain tumor images as Glioma or Mature B cell Lymphomas.

- Foraging gyps africanus optimization (FAGO): The hunting and foraging traits of African vultures and bald eagles served as inspiration for the FAGO algorithm that enhances the convergence speed of the optimization algorithm.
- Foraging gyps africanus optimization enabled distributed explainable AI classifier (FAGO enabled

explainable AI): The integration of the FAGO algorithm with the explainable AI classifier accurately maps the brain tumors. By optimizing the classifier's hyperparameters, the FAGO algorithm lowers the number of local optimal problems and improves the accuracy of brain tumor mapping.

The remaining sections of the articles are organized as follows, section 2 describes relevant works for brain tumor mapping; section 3 discusses the suggested technique for brain tumor mapping using a distributed optimizer explainable AI classifier; section 4 displays the results and discusses the model; and section 5 concludes with the research's future directions.

2. Literature review

The literature review explores the limitations associated with the prior research employed for brain tumor mapping.

Xu et al.[17] designed a tissue cluster-level graph model (tiscut) for tissue segmentation based on histological images. The graph model initially constructs clusters based on spatial distance which solves the segmentation problems and effectively enhances the efficacy of the model. The tissue model may increase the system complexity and may produce false predictions. Cheung et al.[18] the authors utilized the GLCM features-based histopathological image analysis for brain tumors. The SVM model is employed for brain tumor classification. The model leverages the 12 GLCM and 3 GLRLM image features which improves the classification accuracy. Due to tumor heterogeneity, the performance of the model should be improved, and the SVM training process requires a vast amount of annotated data.

Pei et al.[19] presented a 3D CNN model which utilized histopathology images. The segmentation is processed using the encoding-based 3D-NN which enhances the models' performance. However, the dice score difference between the validation and testing datasets was large due to the data imbalance problem. The ROI extraction increases the computational expensive. Im et al.[20] utilized a DL framework for grading tumors. The authors used a pretrained ResNet 50 V2 framework for Glioma screening which enhanced the grading accuracy. However, the model was prone to overfitting issues and class imbalance problems.

Zadeh Shirazi et al.[21] used a deep CNN model (deep survNet) survival rate classification. The model used histopathological images; the patches are extracted using region of interest extraction which identifies the prominent features present in the image. The model can correctly predict the short and long-survival tumors and identify the new targets for glioblastoma. However, the CNN model may need a vast amount of data for validation and testing also reduces the generalization ability of the model. Vankdothu and Hameed[22] implemented a Recurrent (RCNN) for brain tumor classification, which utilized an improved k-means clustering algorithm that visualizes the regions of tumors. The GLCM features enhance the feature extraction capability of the model. However, the model has some limitations such as complexity, and sensitive to local image structures.

Sharif et al.[23] designed a classification model using a multiclass SVM classifier. The pre-trained Densenet201model is utilized for feature extraction; the feature selection process was carried out using two different techniques such as Entropy-Kurtosis-based High Feature Values (EKbHFV) and genetic algorithm (MGA) which selects the optimal features. The major limitation associated with this research is the reduction of important features that impact the classification accuracy. Mudda et al.[24] designed a brain tumor detection model based on textual features. The integration of GLRLM and CS-LSP features identifies the textural relationships between the pixels in the input image that enhance the model's performance. However, the use of a Feed-Forward Back Propagation NN may be prone to overfitting issues.

Challenges

- The unsupervised segmentation methods did not use ground truth images which constrained the number

3

of unique cluster labels.

- An SVM classifier relies on the quality of the data; noise or undesired features in the input image could potentially impact the classification accuracy. Additionally, the GLCM and GLRLM features may increase computational expenses.
- The k-means clustering algorithm was sensitive to initial conditions which cannot handle the Categorical Data.
- Pre-trained Densenet201 lacks explicit domain-specific knowledge, which limits its ability to provide meaningful insights.
- The 3D CNN model can be computationally intensive; due to the data imbalance problem, the dice score difference between the validations and testing datasets was large.

3. Proposed method for brain tumor mapping using distributed optimizer based explainable AI classifier
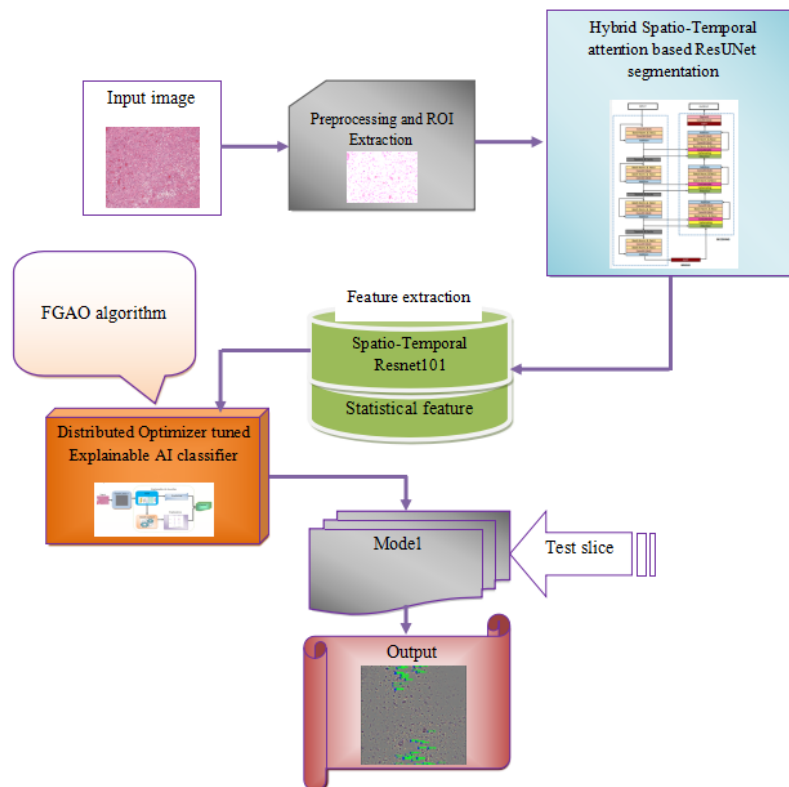

Figure 1. Block diagram of distributed optimizer tuned explainable AI classifier for brain tumor mapping model.

Brain tumors remain a global health concern which increases the mortality rate, early detection and accurate classification are prominent to improve the survival rates and minimize long-term complications. Numerous kinds of research were developed for brain tumor mapping using various imaging techniques. Few researchers only utilized histopathological images for brain tumor mapping; but there are several limitations with the traditional methods such as overfitting and data imbalance. Additionally, the DL classifiers increase the system's complexity. To tackle these issues the paper proposed a distributed optimizer tuned explainable AI classifier for brain tumor mapping. Initially, the histopathological images were collected from the TCGA database. The input images are subjected to preprocessing and region-of-interest (ROI) extraction. The extracted images are subjected to a hybrid spatio-temporal attention-based ResUNet segmentation which produces accurate visualization of brain tumor regions and also increases the segmentation accuracy. The segmented images are further provided as input to the feature extraction process, which extracts the statistical features, and contributed spatio-temporal ResNet-101-based feature flow-based features. The

4

explainable AI classifier, which is built on a distributed optimizer, receives the features and uses the FAGO algorithm to optimize its tunable parameters. The trained model is tested through test slices and the model produces precise output of brain tumor maps. The block diagram of the model is depicted in **Figure 1**.

3.1. Input

In this paper, the histopathological images of brain tumors are collected from the database (256, 256.3) is provided as input to the model,

$$S = \{H_1, H_2, \ldots, H_n\} \tag{1}$$

where S represents the database and $\{H_1, H_2, \ldots, H_i, \ldots, H_n\}$ represents the total number of images present in the dataset.

3.2. Pre-processing and ROI extraction

For medical imaging tasks preprocessing is an essential step that improves the image quality. In this paper for brain tumor mapping the input image is preprocessed using image enhancement technique. Image enhancement aims to enhance the content visibility of the image[25], by adjusting the brightness and contrast the quality of the histopathological image will be increased. Additionally, ROI extraction is performed in this stage which reduces the feature extraction time and identifies the most relevant tumor region. The preprocessed image is denoted as H_i^* which has the dimension of (256, 256,3).

3.3. Hybrid spatio-temporal attention (STA)-based ResUNet segmentation

The process of segmenting the input image into distinguishable sections that are important for tumor mapping is known as segmentation. In this paper, the hybrid spatio-temporal attention-based ResUNet model is utilized for segmentation which improves the robustness of the model. The segmentation technique leverages the advantages of spatio-temporal attention along with the ResUNet model. The conventional segmentation methods have some limitations such as time complexity, and sensitive to noises present in the image. Additionally, prior segmentation methods may struggle with low-quality images such as artifacts, shadows, and non-uniform backgrounds may reduce the effectiveness of segmentation. To tackle these drawbacks the paper introduces a hybrid STA-based ResUNet model. The utilization of UNet along with the Residual blocks addresses the degradation problems. The deep residual units incorporated in this paper make the deep network easy to train and the skip connections enable the propagation of information without degradation[26]. The residual block consists of multiple parallel atrous convolutions with different dilation rate that enables a better understanding of scales. The integration of the spatiotemporal attention layer in ResUNet enhances the feature extraction capability of the model. The architecture of the Hybrid Spatio-Temporal attention-based ResUNet segmentation is illustrated in **Figure 2**. The hybrid STA-based ResUNet segmentation model is an encoder-decoder paradigm that consists of 6 convolutional layers followed by a STA layer in an encoder path. Followed by the convolutional layer the spatio-temporal attention layer is employed to extract relevant features. Followed by the attention layer the residual blocks are employed which eliminates the vanishing gradient and exploding gradients[27].

The input image (256, 256,3) is fed into the convolutional 2D layer which has the filter size 16 and kernel (1×1), the extracted features l_{ab} are provided into the spatial-temporal attention layer $(1 \times 1 \times 3 \times 16)$, the spatial attention mechanism calculates the dynamic weighted sum of the local features $\{l_{a1}, \ldots, l_{an}\}$ the spatial local feature is $\phi[L]$ calculated as[28]:

$$\phi_a[L] = \sum_{a=1}^{n} \alpha_{ab}^{(t)} l_{ab} \tag{2}$$

where $\alpha_{ab}^{(t)}$ represents the spatial attention weights, to calculate attention weights the local features are normalized using the following equation:

$$\alpha_{ab}^{(t)} = \exp\{e^{(t)}{}_{ab}\} / \sum_{b=1}^{n} \{e^{(t)}{}_{ab}\} \tag{3}$$

$$e^{(t)}{}_{ab} = w_l^T \tanh\left(W_e k_{t-1} + U_e v_{l_{ab}} + z_e\right) \tag{4}$$

where represents the previous layer output, w_l^T, W_e, U_e denotes the weights, and the bias is represented as z_e. The spatial attention mechanism helps the decoder to selectively catch the relevant regions concerning the increasing attention weights.
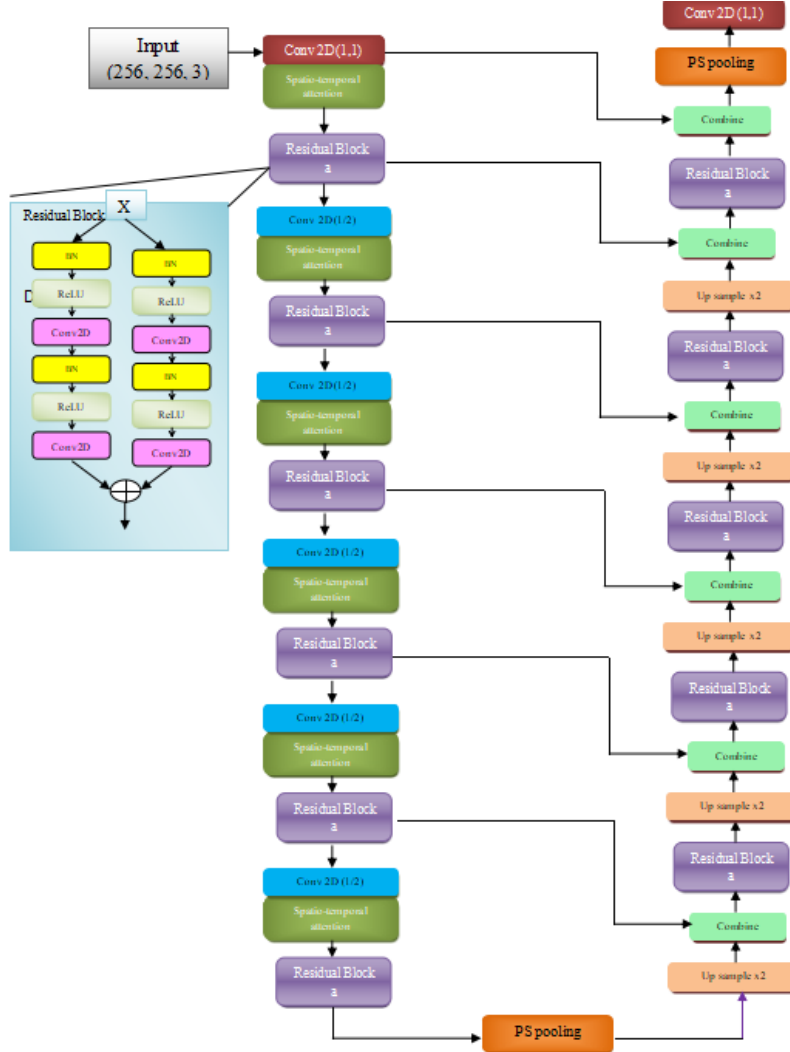

Figure 2. Hybrid spatio-temporal attention based ResUNet segmentation.

Temporal attention is employed to calculate the dynamic global and local features,

$$\varphi_t(VG) = \sum_{a=1}^{d} \beta_a^{(t)} v g_a \tag{5}$$

$$\varphi_t(VM) = \sum_{a=1}^{d} \delta_a^{(t)} v m_a \tag{6}$$

$$\varphi_t(\phi_a[L]) = \sum_{a=1}^{d} \gamma_a^{(t)} \phi_a[L] \tag{7}$$

where $\beta_a^{(t)}, \delta_a^{(t)}, \gamma_a^{(t)}$ are represented as temporal attention weights, the temporal features are fused using the following equation:

6

$$\varphi_t(V) = \varphi_t(VG) + \varphi_t(VM) + \varphi_t(\phi_a[L]) \tag{8}$$

Finally, each will be provided as input to the residual blocks of $[1 \times 1 \times 3 \times 16]$.

The extracted features provided into the residual blocks which consist of batch normalization and ReLU activation functions. The proposed architecture consists of 6 convolutional and spatiotemporal attention layers. After the encoder path, a PS pooling operator is employed. The first input is divided into four equal parts in channel (feature) space by the PSP Pooling operator. The execution of the maximum pooling function in consecutive input layer splits, namely in 1, 4, 16, and 64 partitions. The up sampling procedure in the decoder section is carried out by the nearest neighbor's interpolation, which is followed by a normed convolution with a kernel size of 1. The network's resolution is increased via the batch normalization layer to prevent the segmentation mask's chequerboard artifact. The segmented image $[1,256, 256,3]$ is represented as H_i^S

3.4. Feature extraction

Feature extraction is a fundamental task for image analysis models, in this paper, the following statistical and spatio-temporal ResNet101 features are extracted from the histopathological brain tumor images.

3.4.1. Spatio-temporal ResNet101

The paper proposed a novel feature extraction technique known as spatio-temporal ResNet101, which combines the advantages of the spatio-temporal attention mechanism with the pre-trained ResNet101 model. The spatio-temporal ResNet101 selects significant key frames and features from the image in an adaptive manner with the goal of enhancing the models feature extraction capability. The architecture of the spatio-temporal ResNet101 is depicted in **Figure 3**. The input with the dimension of $[1,256, 256,3]$ is fed into the convolutional layer. To maintain the temporal complexity for each layer, ResNet divides the feature map size in half and adds twice as many filters to the layers with the same output feature map size. The architecture uses a stride of two when convolving layers to do down sampling directly. A completely linked layer with SoftMax turned on and a global average pooling layer mark the end of this ResNet[29]. The features extracted from the spatio-temporal ResNet101 are represented as F_R with the dimension of (1×100).
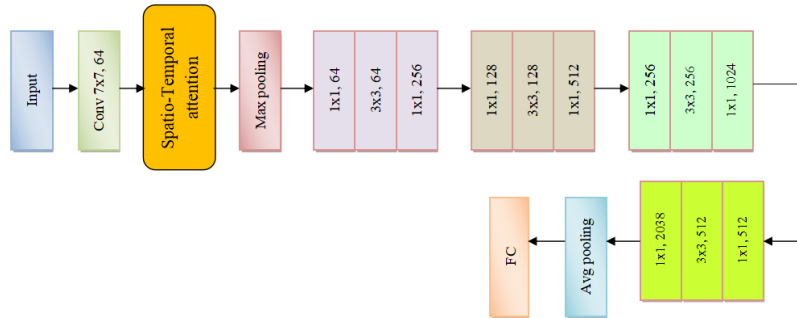

Figure 3. Spatio-temporal ResNet101 architecture.

3.4.2. Statistical features

The statistical features such as mean, variance, standard deviation, kurtosis, skewness, and entropy features are extracted from the segmented images[30], which are mathematically discussed as follows:

a) Mean (μ_B): The average of the image's pixel values is determined by a measurement called mean, which can be calculated as:

$$\mu_H = \sum_{c=1}^{u} \sum_{d=1}^{v} \frac{q(c,d)}{uv} \tag{9}$$

where the pixel intensity value of the pixel (c,d) is represented as $q(c,d)$, uv represents the window size.

b) Standard deviation (σ_B): The measure of the mean distance between the pixel value and the mean is called the standard deviation.

$$\sigma_B = \sqrt{\sum_{c=1}^{u}\sum_{d=1}^{v}\frac{q(c,d)-\mu_B)^2}{uv}} \tag{10}$$

c) Variance (V): variance is defined as the mean of the squared deviations between each pixel value and the mean value.

$$V = \frac{1}{n}\sum_{c=1}^{n}(H_i^S - \mu_B) \tag{11}$$

where a number of samples are represented as n, H_i^S denotes the input.

d) Skewness: Skewness (S_K) is defined as a metric that evaluates the asymmetry in the distribution of pixel intensity.

$$S_K = \frac{1}{n}\sum_{c=1}^{n}\frac{(H_i^S - \mu_B)^3}{\sigma_B^3} \tag{12}$$

e) Kurtosis (K_B): kurtosis is the stability of the distribution which can be calculated as:

$$K_B = \frac{n(n+1)}{(n-1)(n-2)(n-3)}\sum_{c=1}^{n}\frac{\left(H_i^S - \mu_B\right)}{\sigma_B^4} - 3 \tag{13}$$

f) Entropy (E_n): The randomness or uncertainty in the texture is measured using entropy.

$$E_n = \sum_{c=1}^{u}\sum_{d=1}^{v}q(c,d)\log_2 q(c,d) \tag{14}$$

The statistical features are concatenated as $[F_S = \mu_B\|\sigma_B\|V\|S_K\|K_B\|E_n]$ with the dimension $[1 \times 9]$ of the statistical and spatio temporal ResNet101 features $[1 \times 109]$ is fed into the explainable AI classifier.

3.5. Distributed optimizer tuned explainable AI classifier for brain tumor mapping

The distributed optimizer-tuned explainable AI classifier for brain tumor mapping aims to make AI systems' decision-making processes transparent and intelligible. An AI model called XAI is designed to make decisions, reasoning, and goals understandable to the average end user. In this paper, the distributed optimizer-tuned explainable AI classifier integrates the power of both explainable AI and the CNN architecture for brain tumor prediction and classification reduces the biases, and enhances accuracy. **Figure 4** illustrates the architecture of the distributed optimizer-tuned explainable AI classifier. Initially, the input image is provided into the Grad CAM++ which calculates the gradients that produce a better visual representation of predictions[31], the saliency map generated from the is mathematically represented as:

$$H_{c,d}^q = relu\left(\sum_l w_l^q M_{c,d}^l\right) \tag{15}$$

where M^l represents the visualization of l-th the feature map, and q represents the class, w_l^q represents the weights.

The saliency map generated from Grad CAM++ with the dimension of $[1 \times 109 \times 1 \times 1]$ is fed into the CNN model which contains convolutional, pooling, and fully connected (FC) layer. The convolutional layers are utilized for feature extraction and the dimensionality reduction is performed using pooling layers. The final stage CNN is represented by the high-level abstraction that the FC layers produce after receiving the mid- and low-level information. The SoftMax activation function is used to provide the classification scores. Every score for a particular occurrence specify the likelihood of a particular brain tumor[32]. The weight-

sharing feature of CNN lowers the quantity of trainable network parameters, which improves generalization and prevents overfitting. The model output is extremely structured and dependent on the retrieved features due to the concurrent learning of the feature extraction and classification layers.

The generated feature scores are also provided to the SHAP model which is the well-known explainable AI technique that describes the results of machine learning models and is called SHapley Additive exPlanations (SHAP). The model offers a way to gauge how each model component affects a particular data point's outcome which can assist in understanding the features and why a model produced a specific prediction[33]. SHAP calculates the shapely values of features by computing the marginal contributions.

$$\varphi_{F_f}^m = \hat{f}\left(z_{+F_f}^m\right) - \hat{f}\left(z_{-F_f}^m\right) \tag{16}$$

where the marginal contribution with the feature F_f is represented as $\hat{f}\left(z_{+F_f}^m\right)$, and marginal contribution without the feature F_f is denoted as $\hat{f}\left(z_{-F_f}^m\right)$, shapely value is calculated for the input data point p is described as:

$$\varphi_{F_f}(p) = \frac{1}{N}\sum_{m=1}^{N}\varphi_{F_f}^m \tag{17}$$

Through the application of SHAP, model insights can be translated into predictions, enabling the identification and correction of biases, improving performance, and fostering end-user confidence[34]. The SHAP library explains the prediction made by the CNN model; the CNN provides output prediction of two classes named Glioma or Mature B cell Lymphomas. The classifier parameters are tuned using the FGAO algorithm.
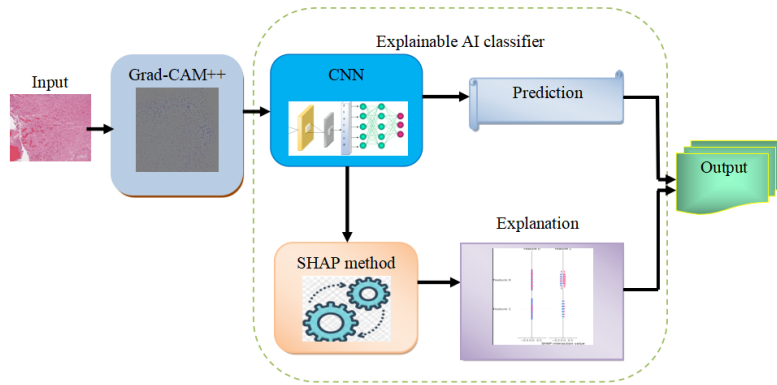

Figure 4. Distributed optimizer tuned explainable AI classifier architecture.

3.6. Foraging gyps africanus optimization algorithm

Motivation:

The FGAO algorithm draws inspiration from the foraging traits of bald eagles[35] along with the navigation and living characteristics of vultures[36]. The algorithm avoids local convergence problems while improving brain tumor mapping and fine-tuning the classifier's tunable parameters.

Inspiration:

The bald eagle follows a unique strategy for foraging which acts as inspiration for the algorithm. The eagles choose a search region during the first phase of their search. During the second phase, the eagles scour the designated area for food. The eagles select and strike a victim during the third stage. Bald eagle movement in all three phases is dependent upon a central location. The eagles travel from the center point to the designated search area in the first phase. The eagles search the area surrounding the center point and inside the search space in the second phase. In the third phase, the eagles take off from the search area's

9

center and fly in the direction of their prey[37]. The navigation and living traits inspired by the gyps africanus (also known as African vultures), based on the circular movements in the sky, the vultures constantly travel to get better food sources. The quality position of the vultures' is obtained by the optimal value of the feasible solutions'; the best and first vulture is identified as the best solution; the second best vulture is defined as second solution. Specifically, all vultures are located nearer to other vultures to avoid local optimum. The combined algorithm enhances the mapping accuracy of the explainable AI classifier.

Initialization:

The tunable classifier parameters such as weights and biases are initialized in this phase which is represented as P^t.

Fitness evaluation:

In this phase, each individual solution in the population has its fitness value, and the fitness function is used to determine which solution is optimal. The fitness function is calculated as:

$$Fit(P^t) = \max(\text{accuracy}(P^t)) \tag{18}$$

Parameter update:

The parameters of the algorithms are updated based on the following stages.

Case (i): Boundary selection $R < 0.5$.

The search lies within the search boundary and the peculiar idea is there is a need for a best position within the boundary to execute the search. This is necessary because eagle needs energy for food hunt which cannot be lost due to the wrong selection of search space.

$$P^{t+1} = P_{p_j\text{best}}^{(t-z)} + \varepsilon_1 \times r(P_{\text{mean}}^t - P_j^t) \tag{19}$$

where $P_{\text{best}}^{(t-z)}$ represents the best solution based on past experience, the current position of the eagle is represented as P_j^t, r is the random number $[0, -1]$, and the constant parameter is denoted as ε.

Case (ii): Knowledge sharing $R \geq 0.5$.

In this phase, the solution executes the search based on the permanent knowledge-sharing phenomenon from neighbors.

$$P^{t+1} = P^t + r_2 s_2(P_h^t - P_j^t) + r_3 s_3(P_{Pj\text{best}}^t - P_j^t) - r_4 s_4(P_{g\text{best}}^t - P_j^t) + \varepsilon_2 P_j^{t-1} + \varepsilon_2(1 - \varepsilon_2)P_j^{t-2} + \frac{1}{6}\varepsilon_1(1 - \varepsilon_2)(1 - \varepsilon_2)P_j^{t-3} \tag{20}$$

The movement of the vulture ε_1 and ε_2 are calculated as:

$$\varepsilon_1 = P_{1\text{best}(j)}^t - \frac{P_{1\text{best}(j)}^t \times K(j)}{P_{1\text{best}(j)}^t - K(j)^2} \times f$$
$$\varepsilon_2 = P_{1\text{best}(j)} - \frac{P_{2\text{best}(j)}^t \times K(j)}{P_{2\text{best}(j)}^t - K(j)^2} \times f \tag{21}$$

where f represents the rate of vulture satiation, current vector position is denoted as $K(j)$, $P_{1\text{best}(j)}^t$ and $P_{2\text{best}(j)}^t$ represents the first and second best solutions in the current iteration. The rotational flight is calculated using the following equations:

$$s_3 = P_{Pj\text{best}}^t \times \left(\frac{rand_5 \times K(j)}{2\pi}\right) \times \cos(K(j)) \tag{22}$$

$$s_4 = P_{Pj\text{best}}^t \times \left(\frac{rand_6 \times K(j)}{2\pi}\right) \times \cos(K(j)) \tag{23}$$

where $rand_5$ and $rand_6$ represents the random number between 0 and 1.

$$s_2 = fit(P_g) + fit(P^t{}_{j1,\text{global}}) \tag{24}$$

where $fit(P_g)$ represents the fitness of the global solution and the fitness of the neighbors best solution is represented as $fit(P^t{}_{j1,\text{global}})$.

Case (iii): Exploitation $R > 1$.

Looks for a better search limit outside the present boundary to explore more valid solutions, the eagle is aware of food abundance and recursive attacks from enemies.

$$P^{t+1} = \frac{P_{\text{worst}} + P_{\exp}^{t-1^{t-2}}}{3_{pj\text{best}_{1_1}}(P_g - P^t)} \tag{25}$$

where $s_1 \in (-1,1)$ represents the boundary searching limits. After this condition, the fitness of the solution is reevaluated. The algorithm iteratively searches for the best solution until the termination criteria are fulfilled. **Figure 5** depicts the flowchart of the FGAO algorithm.
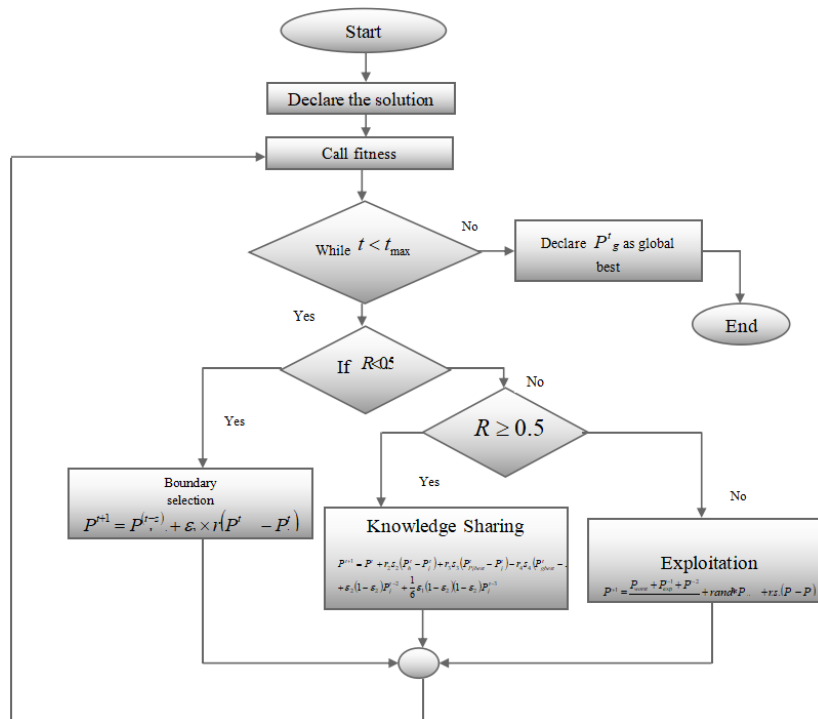
Figure 5. The flowchart of the FGAO algorithm.

4. Results and discussion

The experimental outcomes and performance evaluation of the FGAO-enabled explainable AI for brain tumor mapping are discussed as follows.

4.1. Experimental setup

The execution of the FGAO-enabled explainable AI model is carried out in PYTHON software with 16GB RAM in windows 10 Operating systems.

4.2. Dataset description

TCGA dataset[38]: The dataset consists of histopathological images in two different types of slides which contain a total of 30,036 slides for brain tumors.

4.3. Performance metrics

Accuracy: Accuracy is proportion of accurately mapped brain tumors to the total number of mappings

11

the model made.

$$\text{Accuracy} = \frac{B_p + B_N}{B_p + B_N + B_P + B_N} \tag{26}$$

Sensitivity: The proportion of accurately mapped brain tumors to the positive cases is defined as sensitivity which can be calculated as:

$$\text{Sensitivity} = \frac{B_P}{B_P + B_N} \tag{27}$$

Specificity: Specificity is defined as the ratio of correctly detected non-tumor maps to all negative cases.

$$\text{Specificity} = \frac{B_N}{B_N + B_P} \tag{28}$$

4.4. Experimental outcomes

The experimental image results of the FGAO-enabled explainable AI for the brain tumor mapping model are deliberated in **Figure 6**.
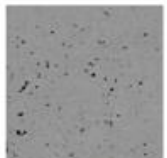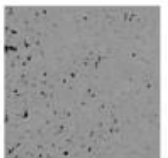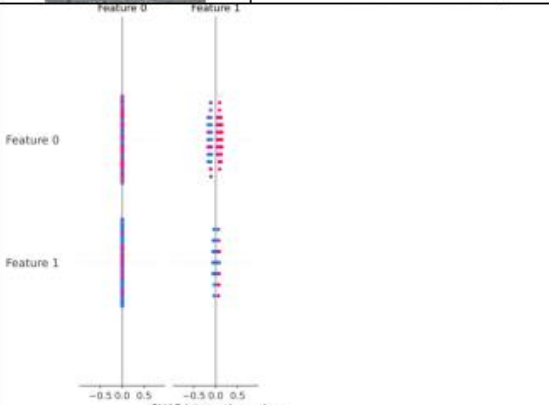
Figure 6. Experimental outcomes of FGAO-enabled explainable AI model.

The disease mapped image obtained using the FGAO-enabled explainable AI is depicted in **Figure 7**.

12

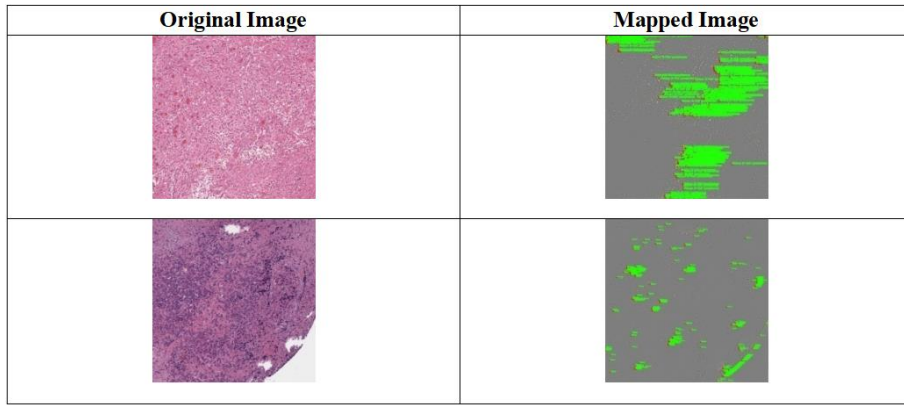| Original Image	Mapped Image

Figure 7. Mapped results of FGAO-enabled explainable AI model.

4.5. Performance analysis

4.5.1. Performance analysis with TP

The performance analysis of the FGAO-enabled explainable AI model with TP for the corresponding epochs is depicted in **Figure 8**. The FGAO-enabled explainable AI model attains an accuracy of 92.64%, 93.09%, 94.04%, 95.37%, and 95.75% for epochs 20, 40, 60, 80, and 100. The sensitivity of the FGAO-enabled explainable AI model for the epochs 20, 40, 60, 80, and 100 is 92.64%, 93.49%, 92.69%, 94.31%, and 95.10% respectively. Similarly, the FGAO-enabled explainable AI model obtains the specificity for brain tumor mapping are 92.64%, 93.52%, 95.47%, 96.18%, and 96.32% for the respective epochs.
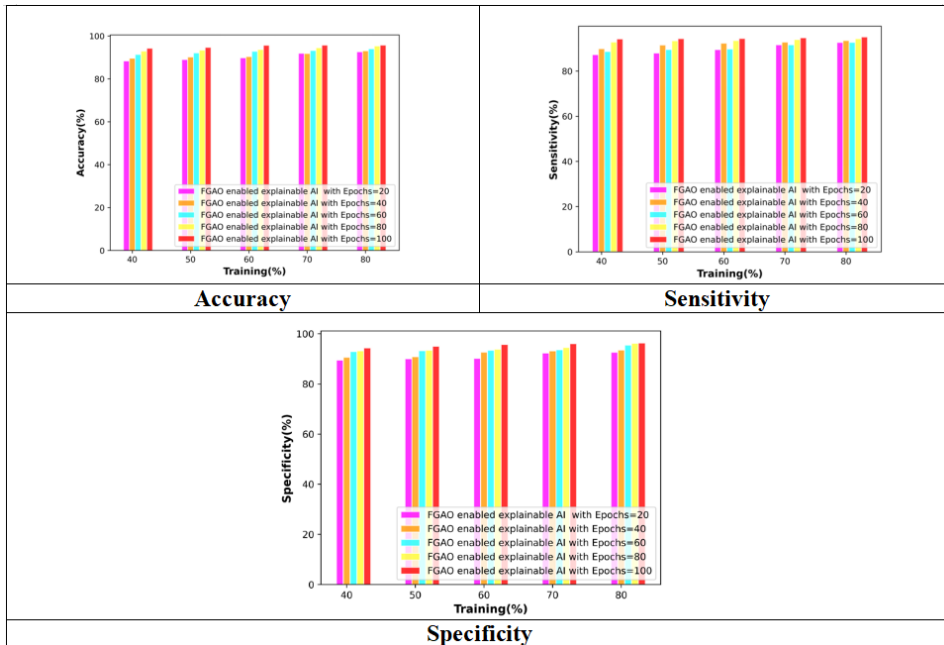

Accuracy	Sensitivity

Specificity

Figure 8. Performance analysis with TP.

4.5.2. Performance analysis with k-fold

Figure 9 depicts the performance analysis of the FGAO-enabled explainable AI model for brain tumor mapping with k-fold value 10. The FGAO-enabled explainable AI model attains an accuracy of 91.75%, 92.94%, 94.47%, 95.59%, and 95.64% for epoch 20, 40, 60, 80, and 100. The sensitivity of the FGAO-enabled explainable AI model for the epochs 20, 40, 60, 80, and 100 is 91.07%, 92.21%, 93.97%, 94.16%, and 94.99% respectively. Similarly, the FGAO-enabled explainable AI model obtains the specificity for brain tumor mapping are 92.44%, 93.70%, 94.98%, 96.48%, and 96.66% for the respective epochs.
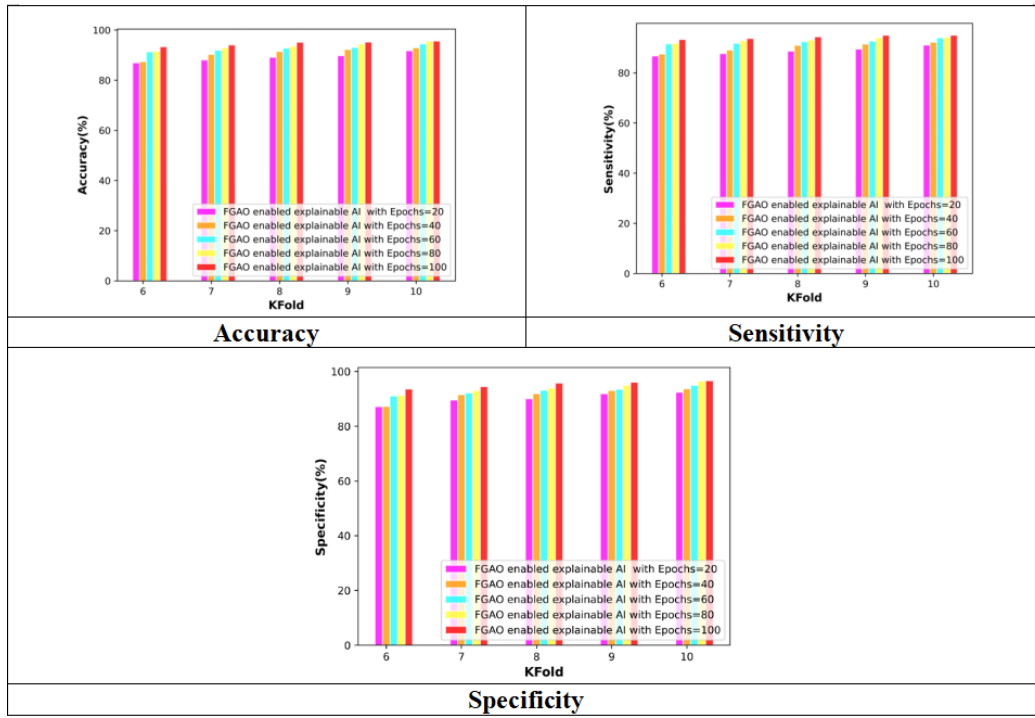
Figure 9. Performance analysis with k-fold.

4.6. Comparative methods

The brain tumor mapping models performance is compared with the traditional techniques such as artificial neural network (ANN)[39], CNN, principle component analysis-long short term memory (PCA-LSTM)[40], deep CNN, explainable AI classifier[41], AVO based explainable AI classifier, BEO based explainable AI classifier.

4.6.1. Comparative analysis with TP

Figure 10 depicts the comparative analysis of the FGAO-enabled explainable AI model with conventional approaches with TP 80. The accuracy obtained by the FGAO-enabled explainable AI model for TP 80 is 95.75% which demonstrates 11.33% improvement over the conventional ANN, 11.29% over CNN, 9.72% over PCA-LSTM, 10.98% over deep CNN, 9.51% over explainable AI classifier, 7.69% over AVO based explainable AI classifier, 4.67% over BEO based explainable AI classifier. The brain tumor mapping model attains a specificity of 95.10% which is far better than the traditional ANN, CNN, PCA-LSTM, deep CNN, explainable AI classifier, AVO-based explainable AI classifier, and BEO-based explainable AI classifier by 16.30%, 14.20%, 11.99%, 13.66%, 9.89%, 9.39%, and 4.80% respectively. The FGAO-enabled explainable AI model for TP 80 obtains a specificity of 96.32% which is improved over the traditional ANN by 11.53%, CNN by 9.92%, PCA-LSTM by 8.29%, deep CNN by 8.78%, explainable AI classifier by 7.68%, AVO based explainable AI classifier by 4.91%, and BEO based explainable AI classifier by 4.44%.

4.6.2. Comparative analysis with k-fold

The comparative evaluation of the FGAO-enabled explainable AI model with the conventional approaches with k-fold 10 is visualized in **Figure 11**. The accuracy obtained by the FGAO-enabled explainable AI model for TP 80 is 95.64% which shows 13.76% improvement over the conventional ANN, 11.97% over CNN, 8.31% over PCA-LSTM, 10.47% over deep CNN, 5.77% over explainable AI classifier, 4.85% over AVO based explainable AI classifier, 5.09% over BEO based explainable AI classifier. The brain tumor mapping model attains a specificity of 94.99% which is far better than the traditional ANN, CNN, PCA-LSTM, deep CNN, explainable AI classifier, AVO-based-explainable AI classifier, and BEO-based explainable AI classifier by 15.41%, 12.58%, 9.40%, 10.80%, 8.89%, 7.23%, and 5.36% respectively.

14

The FGAO-enabled explainable AI model for k-fold 10 obtains a specificity of 96.66% which is improved over the traditional ANN by 12.47%, CNN by 11.69%, PCA-LSTM by 7.58%, deep CNN by 10.48%, explainable AI classifier by 6.72%, AVO based explainable AI classifier by 5.50%, and BEO based explainable AI classifier by 5.17%.
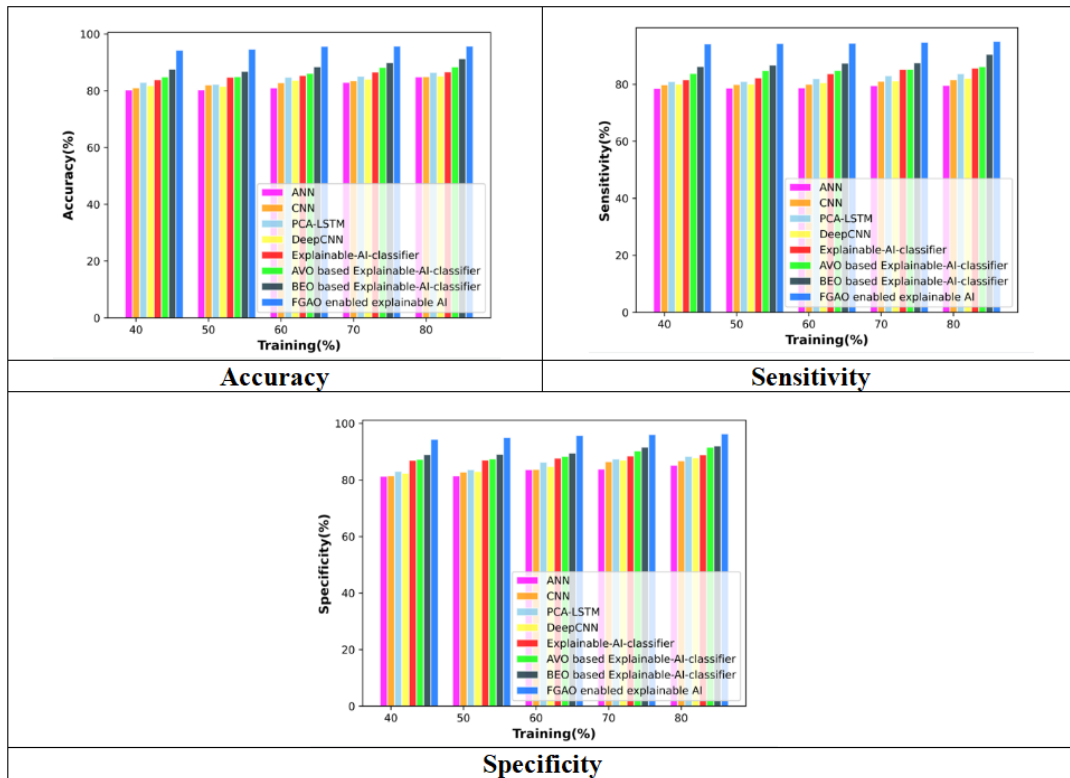

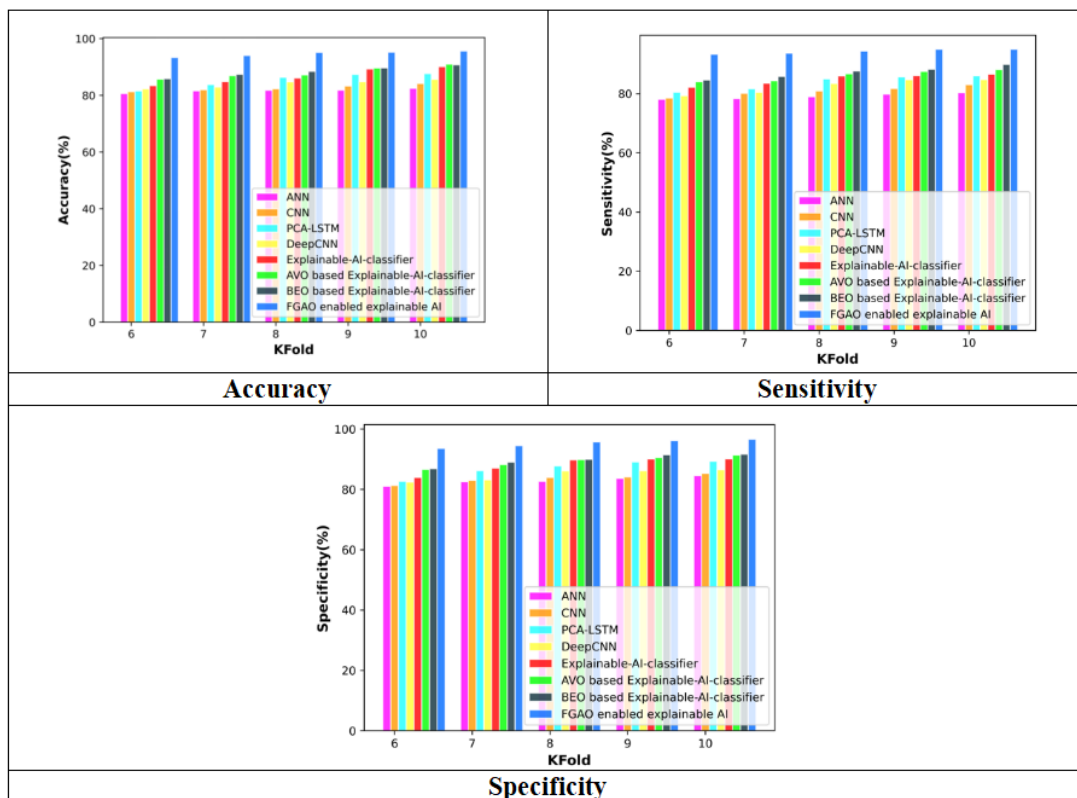
Figure 10. Comparative analysis with TP.

Figure 11. Comparative analysis with k-fold.

4.7. AU-ROC analysis

The AU-ROC analysis of the brain tumor mapping model using FGAO-enabled explainable AI is depicted in **Figure 12**. The analysis shows that when the error decreases performance of the model is increases.
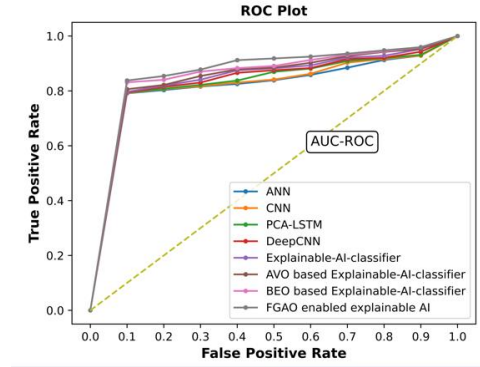

Figure 12. AUC-ROC analysis curve.

4.8. Comparative discussion

The traditional techniques employed for brain tumor mapping have several limitations because brain mapping is patient-specific and cannot be generalized, each patient's brain anatomy is unique, and the functional anatomy may show pathology-induced atypical structure or reorganization. In the PCA-LSTM model errors, including false positives and false negatives, can also be introduced by a variety of factors, such as task design and selection, data collecting, and analysis that limit the models performance. In the ANN model, computational time and scanner availability are the two main practical limitations of the clinical context that affect MRI brain mapping for surgical planning. Selecting and extracting the optimal features from the input image is a challenging task for explainable AI classifiers. To overcome these drawbacks the paper proposed an FGAO-enabled explainable AI brain tumor mapping model that accurately maps the brain tumor as Glioma and Mature B cell Lymphomas. **Table 1** depicts the comparative discussion of the FGAO-enabled explainable AI brain tumor mapping model.

Table 1. Comparative discussion of the FGAO-enabled explainable AI brain tumor mapping model.

Methods	TP 80			K-fold 10		
	Accuracy (%)	Sensitivity (%)	Specificity (%)	Accuracy (%)	Sensitivity (%)	Specificity (%)
ANN	84.90	79.60	85.22	82.48	80.35	84.62
CNN	84.94	81.59	86.77	84.20	83.04	85.37
PCA-LSTM	86.44	83.69	88.33	87.69	86.06	89.34
Deep CNN	85.24	82.10	87.87	85.63	84.73	86.54
Explainable AI classifier	86.65	85.69	88.92	90.12	86.54	90.17
AVO-based explainable AI classifier	88.39	86.16	91.59	91.00	88.13	91.35
BEO-based explainable AI classifier	91.28	90.53	92.04	90.77	89.90	91.67
FGAO enabled explainable AI model	95.75	95.10	96.32	95.64	94.99	96.66

5. Conclusion and future scope

The paper developed a brain tumor mapping model named FGAO-enabled explainable AI which integrates the Dl methods with the explainable AI classifier. The utilization of hybrid spatio-temporal attention-based ResUNet segmentation combines the power of the spatio-temporal attention module and the

ResUNet model that accurately segments the brain histopathological images. The spatio-temporal attention module enhances the model's performance and interpretability. The spatio-temporal attention ResNet101 features extraction model extracts the prominent features from the input image. The integration of an explainable AI classifier along with the SHAP method generates the explanation about the prediction made by the CNN model; which increases the trust between the end user and the AI system. FGAO-enabled explainable AI accurately maps the brain tumor into two classes named Glioma or Mature B cell Lymphomas. The models' performance is compared with the conventional techniques, and the results show that the FGAO-enabled explainable AI classifier attains an accuracy of 95.75%, a sensitivity of 96.10%, and a specificity of 96.32% with TP 80 for the TCGA dataset. Looking ahead, more DL techniques and algorithms will be developed to increase the performance of the model in various domains.

Author contributions

Conceptualization, PRM and NPS; methodology, PNM; software, PRM, NPS and PNM; validation, PRM, NPS and PNM; formal analysis, GRS; investigation, PRM and GRS; writing—original draft preparation, PRM and NPS; writing—review and editing, PRM, NPS, PNM and GRS. All authors have read and agreed to the published version of the manuscript.

Conflict of interest

The authors declare no conflict of interest.

References

1. Tandel GS, Balestrieri A, Jujaray T, et al. Multiclass magnetic resonance imaging brain tumor classification using artificial intelligence paradigm. Computers in Biology and Medicine. 2020; 122: 103804. doi: 10.1016/j.compbiomed.2020.103804
2. Tandel GS, Biswas M, Kakde OG, et al. A Review on a Deep Learning Perspective in Brain Cancer Classification. Cancers. 2019; 11(1): 111. doi: 10.3390/cancers11010111
3. Louis DN, Perry A, Reifenberger G, et al. The 2016 World Health Organization Classification of Tumors of the Central Nervous System: a summary. Acta Neuropathologica. 2016; 131(6): 803-820. doi: 10.1007/s00401-016-1545-1
4. Thaha MM, Kumar KPM, Murugan BS, et al. Brain Tumor Segmentation Using Convolutional Neural Networks in MRI Images. Journal of Medical Systems. 2019; 43(9). doi: 10.1007/s10916-019-1416-0
5. Kotrotsou A, Zinn PO, Colen RR. Radiomics in Brain Tumors. Magnetic Resonance Imaging Clinics of North America. 2016; 24(4): 719-729. doi: 10.1016/j.mric.2016.06.006
6. Davis FG, Malmer BS, Aldape K, et al. Issues of Diagnostic Review in Brain Tumor Studies: From the Brain Tumor Epidemiology Consortium. Cancer Epidemiology, Biomarkers & Prevention. 2008; 17(3): 484-489. doi: 10.1158/1055-9965.epi-07-0725
7. Sharif M, Amin J, Raza M, et al. An integrated design of particle swarm optimization (PSO) with fusion of features for detection of brain tumor. Pattern Recognition Letters. 2020; 129: 150-157. doi: 10.1016/j.patrec.2019.11.017
8. Fernandes SL, Tanik UJ, Rajinikanth V, et al. A reliable framework for accurate brain image examination and treatment planning based on early diagnosis support for clinicians. Neural Computing and Applications. 2019; 32(20): 15897-15908. doi: 10.1007/s00521-019-04369-5
9. Durand T, Bernier MO, Léger I, et al. Cognitive outcome after radiotherapy in brain tumor. Current Opinion in Oncology. 2015; 27(6): 510-515. doi: 10.1097/cco.0000000000000227
10. DeAngelis LM. Chemotherapy for Brain Tumors—A New Beginning. New England Journal of Medicine. 2005; 352(10): 1036-1038. doi: 10.1056/nejme058010
11. Amin J, Sharif M, Yasmin M, et al. Big data analysis for brain tumor detection: Deep convolutional neural networks. Future Generation Computer Systems. 2018; 87: 290-297. doi: 10.1016/j.future.2018.04.065
12. Khan MA, Ashraf I, Alhaisoni M, et al. Multimodal Brain Tumor Classification Using Deep Learning and Robust Feature Selection: A Machine Learning Application for Radiologists. Diagnostics. 2020; 10(8): 565. doi: 10.3390/diagnostics10080565
13. Xu Y, Jia Z, Ai Y, et al. April. Deep convolutional activation features for large scale brain tumor histopathology image classification and segmentation. In: 2015 IEEE international conference on acoustics, speech and signal processing (ICASSP). IEEE. pp. 947-951.
14. Bejnordi BE, Veta M, van Diest PJ, van Ginneken B. Diagnostic Assessment of Dl Algorithms for Detection of

Lymph Node Metastases in Women with Breast Cancer. JAMA. 2017; 318(22): 2199-2210.

15. Madabhushi A, Lee G. Image analysis and machine learning in digital pathology: Challenges and opportunities. Medical Image Analysis. 2016; 33: 170-175. doi: 10.1016/j.media.2016.06.037

16. Xu J, Janowczyk A, Chandran S, et al. A high-throughput active contour scheme for segmentation of histopathological imagery. Medical Image Analysis. 2011; 15(6): 851-862. doi: 10.1016/j.media.2011.04.002

17. Xu H, Liu L, Lei X, et al. An unsupervised method for histological image segmentation based on tissue cluster level graph cut. Computerized Medical Imaging and Graphics. 2021; 93: 101974. doi: 10.1016/j.compmedimag.2021.101974

18. Cheung EYW, Wu RWK, Li ASM, et al. AI Deployment on GBM Diagnosis: A Novel Approach to Analyze Histopathological Images Using Image Feature-Based Analysis. Cancers. 2023; 15(20): 5063. doi: 10.3390/cancers15205063

19. Pei L, Vidyaratne L, Hsu WW, et al. Brain tumor classification using 3d convolutional neural network. In: Brainlesion: Glioma, Multiple Sclerosis, Stroke and Traumatic Brain Injuries: 5th International Workshop, BrainLes 2019, Held in Conjunction with MICCAI 2019; 17 October 2019; Shenzhen, China. Springer International Publishing. pp. 335-342.

20. Im S, Hyeon J, Rha E, et al. Classification of Diffuse Glioma Subtype from Clinical-Grade Pathological Images Using Deep Transfer Learning. Sensors. 2021; 21(10): 3500. doi: 10.3390/s21103500

21. Zadeh Shirazi A, Fornaciari E, Bagherian NS, et al. DeepSurvNet: deep survival convolutional network for brain cancer survival rate classification based on histopathological images. Medical & Biological Engineering & Computing. 2020; 58(5): 1031-1045. doi: 10.1007/s11517-020-02147-3

22. Vankdothu R, Hameed MA. Brain tumor MRI images identification and classification based on the recurrent convolutional neural network. Measurement: Sensors. 2022; 24: 100412. doi: 10.1016/j.measen.2022.100412

23. Sharif MI, Khan MA, Alhussein M, et al. A decision support system for multimodal brain tumor classification using deep learning. Complex & Intelligent Systems. 2021; 8(4): 3007-3020. doi: 10.1007/s40747-021-00321-0

24. Mudda M, Manjunath R, Krishnamurthy N. Brain Tumor Classification Using Enhanced Statistical Texture Features. IETE Journal of Research. 2020; 68(5): 3695-3706. doi: 10.1080/03772063.2020.1775501

25. Singh G, Mittal A. Various image enhancement techniques-a critical review. International Journal of Innovation and Scientific Research. 2014; 10(2): 267-274.

26. Jha D, Smedsrud PH, Riegler MA, et al. ResUNet++: An Advanced Architecture for Medical Image Segmentation. 2019 IEEE International Symposium on Multimedia (ISM). Published online December 2019. doi: 10.1109/ism46123.2019.00049

27. Yan C, Tu Y, Wang X, et al. STAT: Spatial-Temporal Attention Mechanism for Video Captioning. IEEE Transactions on Multimedia. 2020; 22(1): 229-241. doi: 10.1109/tmm.2019.2924576

28. Zhang F, Wang Y, Du Y, et al. A Spatio-Temporal Encoding Neural Network for Semantic Segmentation of Satellite Image Time Series. Applied Sciences. 2023; 13(23): 12658. doi: 10.3390/app132312658

29. Ghosal P, Nandanwar L, Kanchan S, et al. Brain Tumor Classification Using ResNet-101 Based Squeeze and Excitation Deep Neural Network. 2019 Second International Conference on Advanced Computational and Communication Paradigms (ICACCP). Published online February 2019. doi: 10.1109/icaccp.2019.8882973

30. Elazab N, GabAllah W, Elmogy M. Computer-aided Diagnosis System for Grading Brain Tumor Using Histopathology Images Based on Color and Texture Features. Published online August 1, 2022. doi: 10.21203/rs.3.rs-1847884/v1

31. Chattopadhay A, Sarkar A, Howlader P, et al. Grad-CAM++: Generalized Gradient-Based Visual Explanations for Deep Convolutional Networks. 2018 IEEE Winter Conference on Applications of Computer Vision (WACV). Published online March 2018. doi: 10.1109/wacv.2018.00097

32. Alzubaidi L, Zhang J, Humaidi AJ, et al. Review of deep learning: concepts, CNN architectures, challenges, applications, future directions. Journal of Big Data. 2021; 8(1). doi: 10.1186/s40537-021-00444-8

33. Hossain MM, Ali MS, Ahmed MM, et al. Cardiovascular disease identification using a hybrid CNN-LSTM model with explainable AI. Informatics in Medicine Unlocked. 2023; 42: 101370. doi: 10.1016/j.imu.2023.101370

34. Hasan MM, Hossain MM, Rahman MM, et al. FP-CNN: Fuzzy pooling-based convolutional neural network for lung ultrasound image classification with explainable AI. Computers in Biology and Medicine. 2023; 165: 107407. doi: 10.1016/j.compbiomed.2023.107407

35. Alsattar HA, Zaidan AA, Zaidan BB. Novel meta-heuristic bald eagle search optimisation algorithm. Artificial Intelligence Review. 2019; 53(3): 2237-2264. doi: 10.1007/s10462-019-09732-5

36. Abdollahzadeh B, Gharehchopogh FS, Mirjalili S. African vultures optimization algorithm: A new nature-inspired metaheuristic algorithm for global optimization problems. Computers & Industrial Engineering. 2021; 158: 107408. doi: 10.1016/j.cie.2021.107408

37. Wang Y, Li S, Sun H, et al. The utilization of adaptive African vulture optimizer for optimal parameter identification of SOFC. Energy Reports. 2022; 8: 551-560. doi: 10.1016/j.egyr.2021.11.257

38. TCGA database. Available online: http://www.andrewjanowczyk.com/download-tcga-digital-pathology-images-ffpe/ (accessed on 1 December 2023).

39. Amarapur B. An automated approach for brain tumor identification using ANN classifier. In: 2017 International conference on current trends in computer, electrical, electronics and communication (CTCEEC). IEEE. pp. 1011-

1016.

40. Islam MK, Ali MS, Miah MS, et al. Brain tumor detection in MR image using superpixels, principal component analysis and template based K-means clustering algorithm. Machine Learning with Applications. 2021; 5: 100044. doi: 10.1016/j.mlwa.2021.100044

41. Ahmed F, Asif M, Saleem M, et al. Identification and Prediction of Brain Tumor Using VGG-16 Empowered with Explainable Artificial Intelligence. International Journal of Computational and Innovative Sciences. 2023; 2(2): 24-33.